Proceedings of the ASME 2016 35th International Conference on Ocean, Offshore and Arctic Engineering
OMAE2016
June 19-24, 2016, Busan, South Korea

OMAE2016-55008

EXTREME TYPHOON LOADS EFFECT ON THE STRUCTURAL RESPONSE OF OFFSHORE METEOROLOGICAL MAST AND WIND TURBINE

Tsung-Yueh Lin **Yann Quéméner**

CR Classification Society
Taipei, Taiwan (R.O.C.)

ABSTRACT

Recently, Taiwan started to evaluate the potential of wind energy production on its West coast. The concern was raised about employing existing solutions validated by experience for mild environment regions to Taiwan which is frequently subject to Typhoon. This study investigated the strength under typhoon condition of two offshore wind farm units: a meteorological mast supported by a monopile and a 3.6 MW wind turbine supported by a 4-leg jacket. Especially, two critical load cases were analyzed. First, the study provided a simplified approach to evaluate the wave run-up load on a monopile. The dynamic structure response of the meteorological mast evaluated through finite element analyses showed that large vibrations excited the tower after the slamming. In a second time, the study evaluated the extreme wind loads exerted on the blades of the parked wind turbine considering a blade pitch control fault. As a result, for a constant gust wind speed of 70 m/s, the loads at the nacelle increased tremendously by approximately 220% compared to the parked wind turbine without fault condition.

INTRODUCTION

Recently, Taiwan started to evaluate the potential of wind energy production on its West coast. As most of the worldwide experience regarding wind turbine are concentrated on onshore units and offshore with mild environment conditions, the concern was raised about employing existing solutions for Taiwan environment frequently subject to typhoon. Extensive data collection is the key to produce reasonable and safe design load conditions and thus in 2015 three meteorological masts have been installed in the potential wind farms areas. The first full scale test 3.6 MW offshore wind turbine should then be installed in 2016.

This study investigated the strength under typhoon condition of two wind farm units: an 86 m high meteorological mast supported by a monopile and a 3.6 MW wind turbine supported by a 4-leg jacket. Lacking reliable long term typhoon wind and wave data, this study considered a gust wind speed of 70 m/s as reported by and a maximum wave height of 14.9 m in compliance with the Ministry of Economic Affaire (MEA) requirements [1]. Recently, for the West coast of Taiwan, Chang et al [2] conducted analyses to predict statistically design extreme wind speeds at 100 m high (i.e. approximately wind turbine hub height) derived from wind measurements at the ground level, and 70 m/s would be consistent with the extreme gust wind speed obtained for a 50 years return period. Preliminary Metocean data were also made available for the installation site including the significant wave height, and the 14.9 m would be consistent with a maximum wave height for a 100 years return period. Finally, from the Metocean data, an extreme water depth including storm surge was set to 25 m and a surface current speed of 1.4 m/s at was produced.

Accurate typhoon design load evaluations are also required to reduce uncertainties. This study investigated first the wave run-up [12,13] load of non-breaking waves which the effect on the strength would be significant for monopile-supported units and negligible for jacket-supported units. Various certification bodies have addressed guidelines with simplified approaches to evaluate the slamming force of breaking waves. Khansari et al [3] compared 6 guidelines approaches that are validated based on offshore oil and gas experience. This study provided thus a method that employed CFD to calibrate a semi-analytical model similar to those described in [3] to evaluate the wave run-up loads.

This study investigated then the extreme blades wind load exerted on the parked wind turbine considering the fault of the blade pitch control system that would prevent reducing the blade projected area normal to the direction of the wind,

inducing extremely high loads at the nacelle. Various approaches exist such as the time consuming computational fluid dynamic (CFD). However, this study preferred the blade element momentum (BEM) method that is much faster and convenient to evaluate the blades wind loads.

This study consists of three sections. The first section evaluates the wave run-up loads on the monopile foundation of the meteorological mast. The second section assesses the wind loads on the blades exerted on the parked wind turbine considering blade pitch control fault. The third section presents the dynamic structural response of the two wind farm units to the loads produced in the previous sections.

WAVE RUN-UP LOADS ON MONOPILE

The nearshore ocean wave dynamics can be subject to nonlinearity and wave breaking due to the seabed terrain. Various wave theories enable defining analytically the wave flow field of non-breaking waves, whereas the breaking waves can be studied through experiments and hydrodynamic numerical analyses such as CFD. Figure 1 presents the range of validity of regular wave theories provided by DNV [4]. For the design wave considered in this study which the parameters are summarized in Table 1, the flow properties can be evaluated using the nonlinear intermediate-depth 5th-order Stoke's wave theory. Figure 2 presents the wave particles velocity and acceleration at the free surface evaluated applying the 5th-order Stokes wave theory (full line) and the regular Airy wave (dash line). It can be observed that the nonlinear wave velocity and acceleration results in larger amplitudes and steeper variations compared to the linear wave assumption.

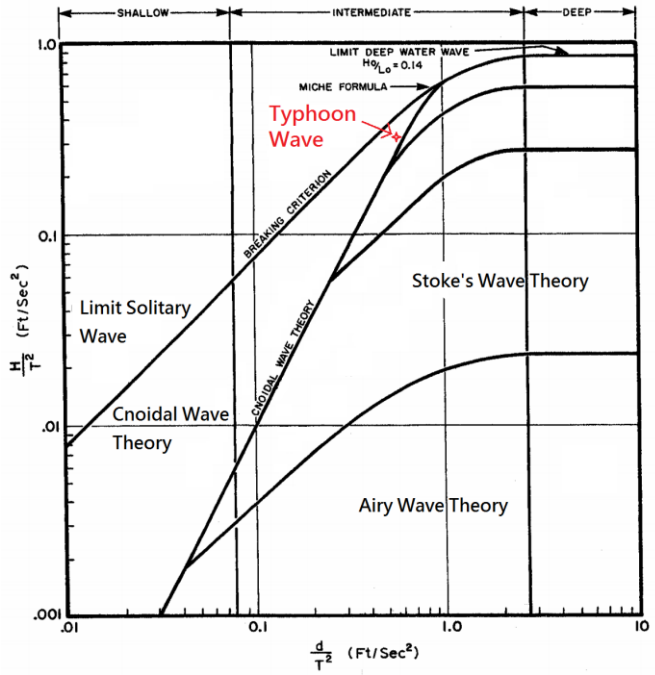

Figure 1. Categories of regular wave theories.

Table 1. Typhoon wave parameters.

Wave Height (m)	14.88
Period (s)	12.47
Wave Length (m)	194
Water Depth (m)	25.03
Current Speed (m/s)	1.4

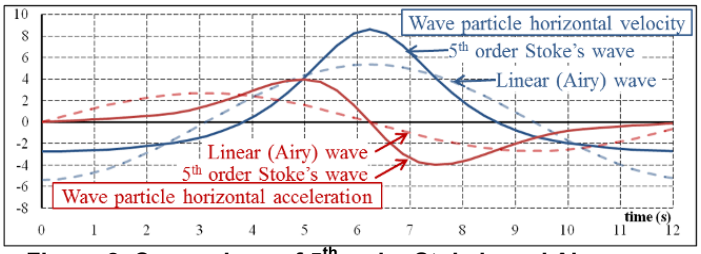

Figure 2. Comparison of 5th-order Stoke's and Airy wave velocity (m/s) and acceleration (m/s^2) at the free surface.

When the wave particles flow is defined, the wave loads on the offshore structure can be produced. A popular and convenient approach to evaluate the wave loads on slender bodies consists in applying the Morison equation [5] provided in Eq. (1), which calculates time-varying loads of slender bodies per unit length (i.e. line loads). The applicability of the equation is limited to non-breaking and regular waves which the length is 100 times longer than the characteristic dimension of the structure; here the diameters of the monopile was about 4 m. The Morison equation divides the wave loads into an inertia and a drag term considering that the flow condition is not significantly disturbed by the structure. The inertia term is proportional to the acceleration of the wave particles, and the drag term relates to the square of the velocity.

$$F_M = \rho_{sw} \cdot C_M \cdot A \cdot \dot{v} + \frac{1}{2} \rho_{sw} \cdot C_D \cdot D \cdot v \cdot |v| + F_S \qquad (1)$$

where ρ_{sw} is the specific gravity of the seawater, C_M is the inertia coefficient set to 2.0 as minimum value recommended by DNV [4] "for structures in shallow waters near coastlines where there is a significant current in addition to the waves", A is the projected area of the monopile, D is the pile diameter, and C_D is the drag coefficient which can be computed according to DNV recommendation [4] that relates, amongst other parameters, to the roughness of the structure and thus to the marine growth, here assumed taking place under the lowest astronomical tide (LAT) water level. For the considered monopile under extreme wave height, the drag coefficient below and above the LAT water level was found equal, approximately, to 1.25 and 0.65 respectively. Finally, the wave particle velocity included the current velocity that followed a power distribution over the water depth from the seabed (V = 0 m/s) to the "calm water" sea surface (V = 1.4 m/s, see Table 1).

This study employed an in-house developed software named HydroCRest that can compute the Morison equation from the wave particles field derived from linear and nonlinear Stokes

and Cnoidal theories waves. To calculate the Morison equation, the velocities and accelerations of water particles at virtual structural nodes are analytically derived from the corresponding theoretical wave [15]. Figure 3 presents the wave sectional load distribution along the monopile at the wave crest. It can be observed that at the wave crest, the drag contribution was approximately twice larger than the inertia component. At the LAT, the drag component of the wave loads dropped abruptly because the marine growth was defined until the LAT, so that at the LAT the drag coefficient decreased from 1.25 to 0.65. Then, at approximately 8 m above the LAT, the drag component of the wave loads dropped again abruptly because the current was defined until the extreme mean water level (MWL) surface, so that above the water depth the current speed was set to zero. It is to be noted that the abrupt sectional loads changes observed at the LAT and at the MWL surface are not realistic. However after integration over the monopile height, the produced structure bending moment distribution would be reasonably accurate.

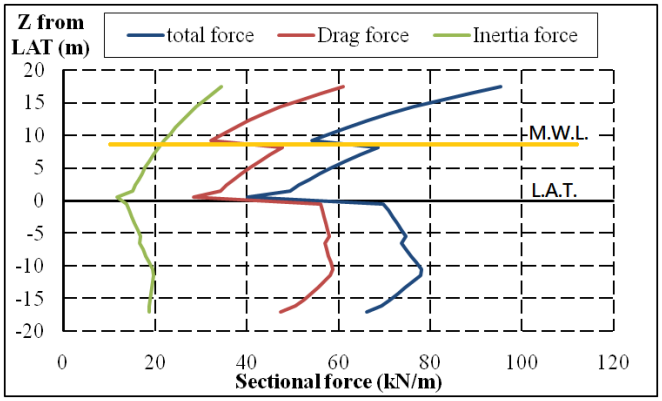

Figure 3. Sectional load distribution along the monopile at the wave crest.

Afterwards, to capture the entire flow-structure interaction phenomenon in extreme regular waves, computational fluid dynamic (CFD) simulations were conducted through Star-CCM+. CFD solves Reynolds-averaged Navier-Stoke's equation for general flow problems. Simulation time was three periods of regular waves, but only the result of the last period were used. The numerical scheme was first order up-wind difference due to the hyperbolic PDE in wave simulations, and the time step was 7.5 ms. Flow domain was meshed by Cartesian and prismatic layer algorithms. Boundaries extended to three times the wave length in the wave propagating direction and ten times the monopile diameter in the transverse direction. The mesh size was of 0.375 m around the structure and 0.15 m in the gravity direction near the wavy free surface. All y+ of realizable k-epsilon turbulence model was used to calculate the turbulent intensity and dissipation. Convergence tests were applied by checking variable residuals down below 10^{-4}. In Fig. 1, it can be observed that the considered wave was close to the breaking limit. As for the Morison equation approach, the flow field of the wave was obtained applying the Stokes theory. However, the CFD can precisely take into account the free surface effect using the volume of fluid (VoF) technique, whereas HydroCRest, under the Morison equation limitations, assumes that the pile does not disturb the wave flow. Finally, to reproduce the perfectly smooth surface of the monopile considered by the CFD analyses and thus enable comparing CFD and HydroCRest results, the drag coefficient in the Morison equation was set to 0.65 accordingly to DNV [4].

Figure 4 presents the comparison of the sectional loads at the crest on the monopile by HydroCRest (full line) and by CFD (dash line). It can be observed that from the seabed till 3 m under the wave free surface, the trend of sectional load distribution obtained by CFD analysis compared well to that reproduced by HydroCRest, but the amplitude was approximately 60% higher. Therefore, the CFD simulations were not able to reproduce the drag force provided by the Morison equations and thus further parametric studies are required to validate the settings used in the CFD analyses. Additionally, in Fig. 4, it can be observed that close to the wave surface, the CFD sectional loads were three times larger than those produced by HydroCRest. In order to isolate that local load increase, the drag coefficient employed in the Morison equation was reduced by 60% (i.e. C_D = 0.4) to match the CFD results below the free surface disturbance area.

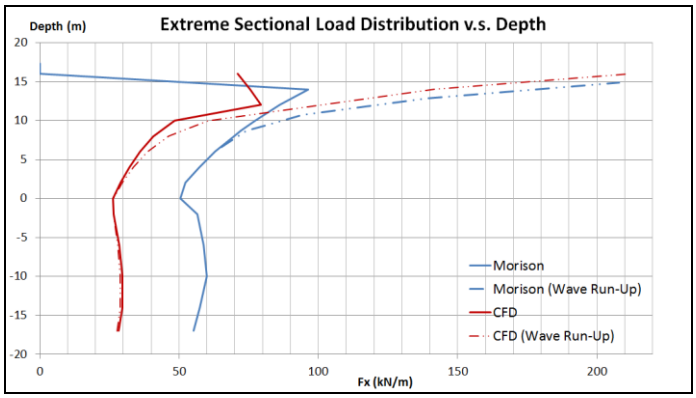

Figure 4. Sectional load distribution along the monopile produced by CFD and by HydroCRest.

Figure 5 presents views from the CFD simulations of the free surface significantly disturbed by the structure at the wave crest. The Morison equation is not applicable for this large free surface disturbance. In Fig. 5, it can be observed that a wave flow is accumulating at the front face of the pile and a water level drop behind the pile. In this study, this phenomenon was identified as the run-up effect also described by the velocity stagnation head theory [14] that leads to the different fluid densities (i.e. water and air) load onto the two sides of a tubular section. The wave run-up effect results in an additional wave load similar to slamming, even though it is a non breaking

wave. This effect comes from the three following properties of an extreme high regular wave:

- very steep free surface of nonlinear waves near the crest,
- very high wave celerity (i.e. wave speed), and
- momentum contracted within the crest.

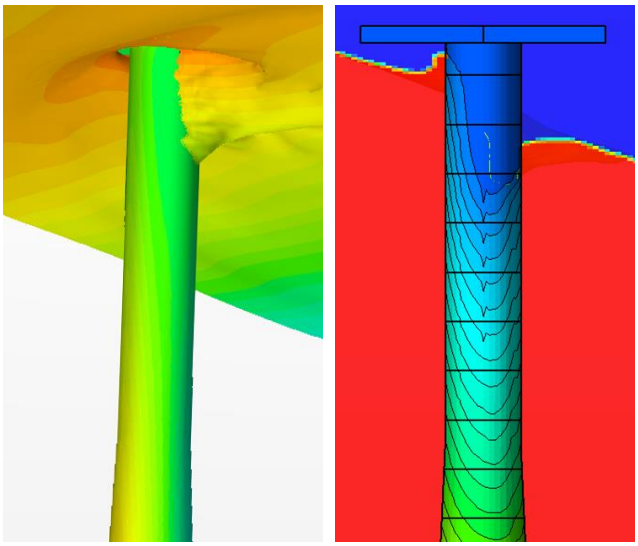

Figure 5. View of the wave run-up effect obtained by CFD.

Although the CFD approach was very precise to capture nonlinear effects, it was also very demanding in time of computation. Therefore, a faster approach was preferred through the addition of a slamming load component F_S in the Morison equation (see Eq. (1)). Khansari and Oumeraci [3] compared existing methods to evaluate the slamming force of breaking waves on pile recommended by several guidelines including DNV [6] that provides the Eq. (2).

$$F_S = \frac{1}{2}\rho_{sw} \cdot C_S \cdot D \cdot v \cdot |v| \tag{2}$$

where v is the wave particle horizontal velocity and C_s is the slamming coefficient that can be computed by Eq. (3).

$$C_S = 5.15\left(\frac{D}{D+19s} + \frac{0.107s}{D}\right) \tag{3}$$

where s is the penetration distance of the wave across the pile diameter. C_s equals 5.15 when the wave crest meets the front face of the pile ($s = 0$) and 0.809 when the wave profile entirely covers the pile section ($s = D$). However, the slamming area needs to be assumed by the designer which may induce large uncertainties.

This study proposed a similar model to Eq. (2) that includes dynamically the slamming area affected by the wave run-up through the Froude number into a C_s formulation provided in Eq. (4).

$$C_S = \frac{P_m}{1+\sqrt{\frac{g}{P_d|v|}\frac{d}{D}}} + \frac{P_m}{2} \tag{4}$$

where d is the water head above the considered section, P_m is the wave run-up magnifier and P_d is the factor for water level drop, that were calibrated based on the CFD results as 3.0 and 2.5 respectively. For a section at the wave surface, d is close to 0 and C_s tends towards $1.5\times P_m$, whereas for section further from the wave free surface, d is very large and C_s tends towards $0.5\times P_m$. The wave run-up depth (see Fig. 6) was already related to the Froude Number in [12,13], and it is the key variable in the model proposed in Eq. (4).

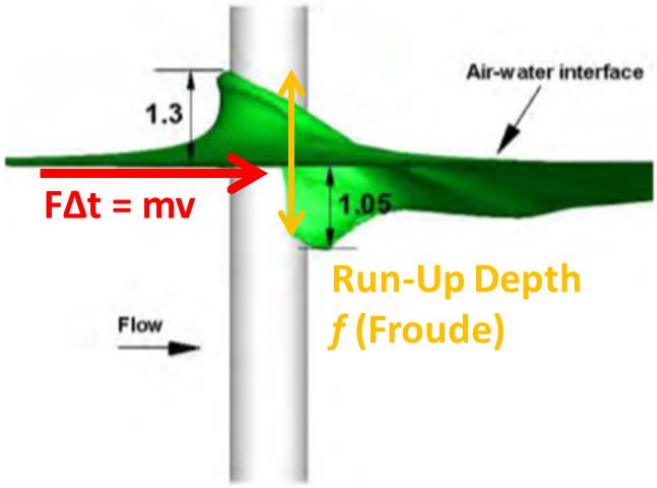

Figure 6. Wave run-up depth defined by Froude Number.

Finally, the approach would be convenient to evaluate the slamming load induced by the wave run-up of a non-breaking wave. However, in order to extract accurate P_m and P_d values, the CFD settings need first to be calibrated to the drag coefficient provided by DNV formulation. The scope of the CFD analyses could also be extended to more monopile diameters and wave height in order to obtain semi-analytical formulations of P_m and P_d.

WIND LOADS FOR A PARKED WIND TURBINE WITH BLADES PITCH CONTROL FAULT

In this study, a blade element momentum (BEM) method was preferred to time consuming computational fluid dynamic (CFD) simulations. Because its maturity, the BEM method is widely being used in the wind turbine design and analysis [16]. The BEM method consists in the combination of the 2D blade element theory and the actuator disk momentum theory. The 2D blade element theory enables calculating the aerodynamic forces, dF_N and dQ, on a blade section profile from its relative inflow velocity U_{rel} (see Fig. 9 (left)), as provided in Eq. (5).

$$dF_N = nB\frac{1}{2}\rho U_{rel}^{\ 2}\left(C_l\cos\varphi + C_d\sin\varphi\right)cdr$$
$$dQ = nB\frac{1}{2}\rho U_{rel}^{\ 2}\left(C_l\sin\varphi + C_d\cos\varphi\right)crdr \quad (5)$$

where φ is the inflow direction and C_l, C_d are the sectional lift and drag coefficients. c and n_B are the chord length of each blade section and the number of blades.

Based on the conservation of momentum, the inflow velocity decreases when passing through the rotor disk by transferring its energy to the blades as illustrated in Fig. 7 (right). The inflow velocity decrease can be computed by the Eq. 6.

$$U_{rel}(r) = \sqrt{U_{hub}^2(1-a)^2 + \Omega^2 r^2(1+a')^2}$$
$$\varphi = \tan^{-1}\left[\frac{U_{hub}(1-a)}{\Omega r(1+a')}\right] \quad (6)$$

where a and a' are the axial and tangential induction factors that can be calculated by the actuator disk theory.

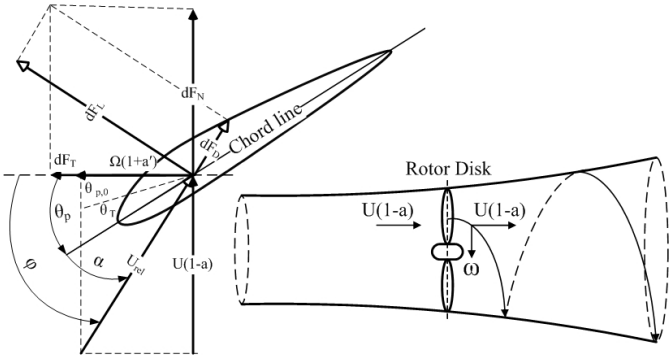

Figure 7. Blade element (left) and actuator disk momentum (right) methods.

Specific corrections were also applied to adapt the BEM method to the turbine blades problem. Tip-loss correction that can gradually reduce loads to zero at the blade tips as the blade is finite in length with only three blades on the rotor disk. Glauert's correction [7] prevents unrealistic flow induction according to experiments measurement. Pitt's correction [8] enables accounting for the skewed wake effect on the flow induction, which is necessary for tilted or yawed rotor conditions.

For validation, the BEM predictions of a 2.0 MW wind turbine were compared to the manufacturer's data [9]. Figure 8 presents the power curve provided by the manufacturer and those evaluated by the BEM method with and without pitch control correction. It can be observed that the predicted power curve was very close to the manufacturer's data for the nominal speed range and also beyond the cut-out wind speed where the pitch control system must engaged.

The detailed design of the considered 3.6 MW wind turbine blades was not available to evaluate the extreme load. This study employed thus a method to deduce the geometry of wind turbine blades from its basic data (e.g. diameter, power, nominal wind speed and nominal rotation speed) through an inverse calculation approach. Figure 9 presents the flowchart of the inverse calculation procedure. First, the blade section profile distribution and chord length were scaled up from a 2.0 MW wind turbine design to the target 3.6 MW turbine blade. The twist angle of each blade section along the blade were then tuned to optimize the lift and thrust, so that the generated blade model can produce the torque and thus the power provided by the manufacturer for the design nominal wind speed and rotor rotation speed. Table 2 presents the deduced blade geometry characteristic per section for the 3.6 MW turbine, as well as the basic input data and target function.

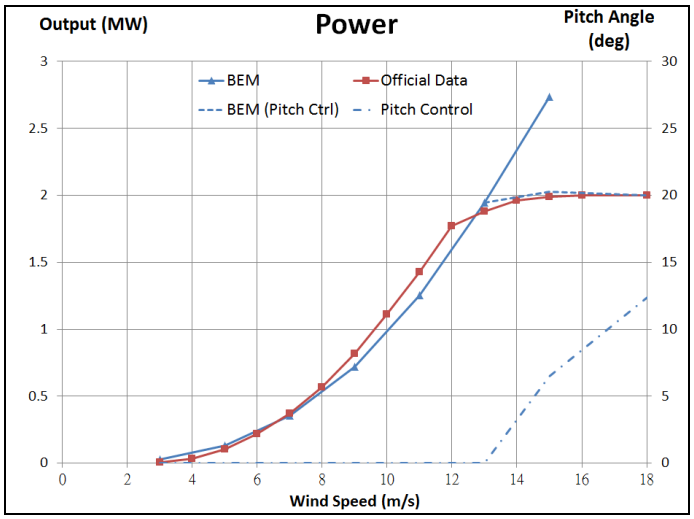

Figure 8. Power curve of 2.0 MW wind turbine by BEM.

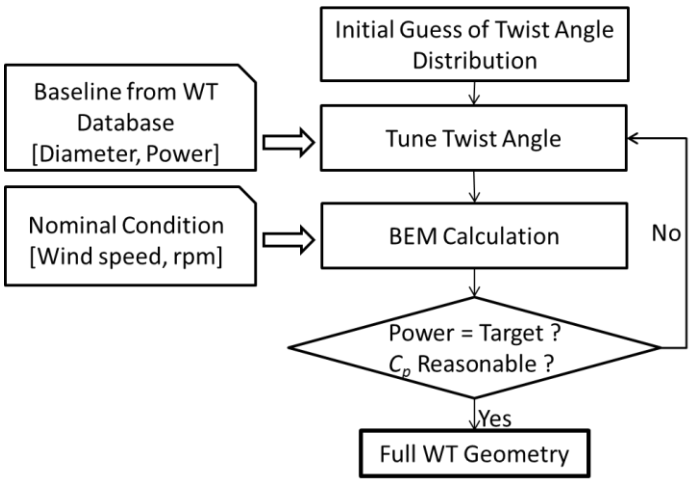

Figure 9. Flowchart of the inverse calculation of BEM.

Table 2. Inverse calculation of 3.6 MW rotor by BEM.

Design Criteria	
Wind Speed	12 m/s
Rotor Speed	13 rpm
Num. Blades	3
Rotor Radius	60 m
Hub Radius	1.5 m
Pitch Angle	0 deg

Target Function
Power = 3.616 MW
Cp = 0.3
Axial Load = 415.6 kN

Index	Radius (m)	Chord Length (m)	Twist (deg)	Section Shape
1	1.600	2.21	3.00	cylinder
2	6.375	3.05	13.00	DU00w-401m2
3	11.250	3.23	12.50	DU00w-350m2
4	16.125	3.01	9.88	DU97w-300
5	21.000	2.74	7.26	DU97w2-250
6	25.875	2.43	4.68	DU93w-210
7	30.750	2.09	2.47	DU95w-180
8	35.625	1.85	1.32	DU95w-180
9	40.500	1.58	0.47	NACA64-3-618
10	45.375	1.31	0.04	NACA64-3-618
11	50.250	1.24	5.75	NACA64-3-618
12	55.125	1.04	0.89	NACA64-3-618
13	59.900	0.44	3.79	NACA64-3-618

The obtained wind load under nominal operation condition was of 416 kN. Then, this study evaluated the wind load exerted on the parked wind turbine for an extreme gust wind speed of 70 m/s considering:

- No blades pitch control fault: rotor stopped, 90 deg blade pitch
- Blades pitch control fault: rotor stopped, 0 deg blade pitch

Table 3 presents the extreme load prediction for the two parked configurations. For the parked wind turbine without fault, the wind load was found equal to 80 kN, whereas for the parked wind turbine with fault the load raised to 2030 kN. The wind load on the tower was calculated by the drag force formulation provided in Eq. (7) that neglects the mutual interaction between the rotor and the tower.

$$F_W(z) = \frac{1}{2}\rho_{air} \cdot C_D \cdot \mathrm{D}(z) \cdot U_w^2(z) \qquad (7)$$

where C_D is the drag coefficient, D is the conical tower diameter and U_w is the wind speed.

Table 3. Wind shear force of an 3.6 MW wind turbine.

Loaded items	Wind Speed	
	12 m/s	70 m/s
Blades - Normal Operation	416 kN	-
Blades – Parked without fault	-	80 kN
Blades - Parked with fault	-	2030 kN
Tower	35 kN	1200 kN

STRUCTURAL ANALYSIS

Finite Element modeling

The meteorological mast's triangular lattice tower and monopile foundation as well as the wind turbine's tower, jacket foundation and piles in soil were modeled using 1D 'Beam' Finite Elements of tubular section and of approximately 1 m length. Figure 10 presents the FE models of the meteorological mast and the wind turbine. The different colors on the structures indicate the different tubular sections employed in the model.

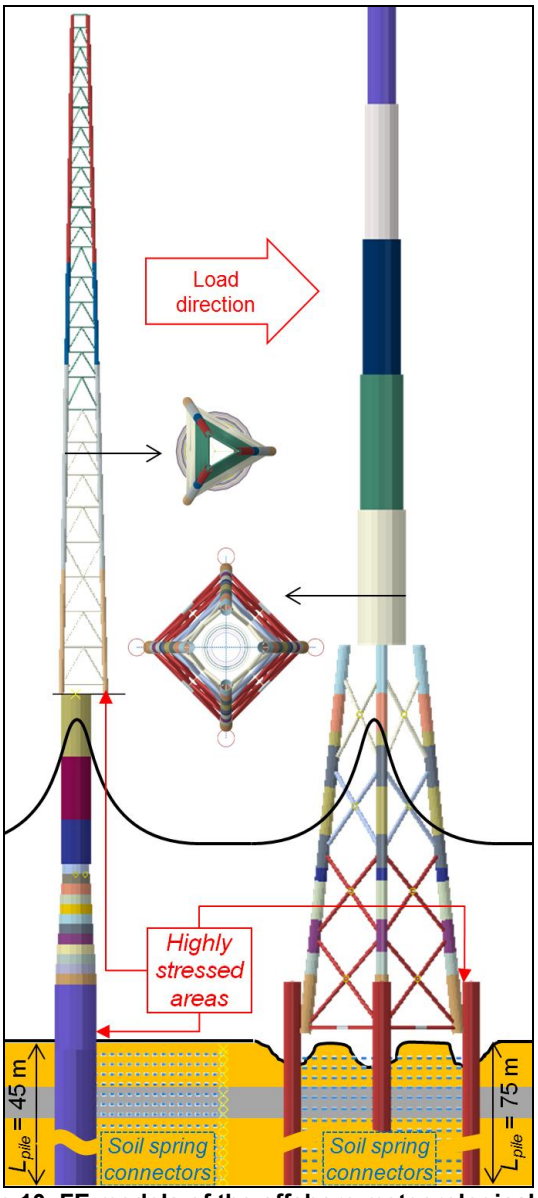

Figure 10. FE models of the offshore meteorological mast (left) and the wind turbine (right).

The material was set as linear elastic with a Young modulus of 210000 N/mm^2 and a Poisson ratio of 0.3. The masses of the equipments and secondary structures (e.g. Nacelle, blades and access platform) were added to the FE models. The soil resistance to the pile lateral and axial displacements was represented through spring connectors which the nonlinear elastic behavior corresponded to the p-y, t-z and q-z curves formulations provided by DNV [10]. For the meteorological mast, because an adequate scouring protection system was provided around the monopile, this study assumed that no scouring would occur at the seabed, whereas for the wind turbine, a 2 m deep scouring was considered at each pile of the jacket foundation. Finally, the loads obtained in the previous sections were applied to the FE models through line loads (i.e.

force per unit length) on the beam elements and a concentrated force for the blades wind loads at the nacelle. As provided by DNV [11] for ultimate strength assessment, a 1.35 load factor was applied on the environmental loads. Finally, explicit dynamic analyses were performed for the four following cases of study:

- Meteorological mast under constant gust wind load and dynamic wave load without wave run-up effect,
- Meteorological mast under constant gust wind load and dynamic wave load with wave run-up effect,
- Parked wind turbine under constant gust wind load considering a blade pitch control fault condition, and dynamic wave load without wave run-up effect, and
- Parked wind turbine under constant gust wind load considering no blade pitch control fault condition, and dynamic wave load without wave run-up effect.

Wave run-up load on monopile

The wave run-up effect on the meteorological mast dynamic structural response was here analyzed. Figure 11 presents the global overturning moment at the seabed exerted by the environmental loads (i.e. wind, wave, current) with and without wave run-up effect consideration. At first, the constant wind load was applied through a 5 s preload step. The dynamic wave loads were then applied during three wave periods.

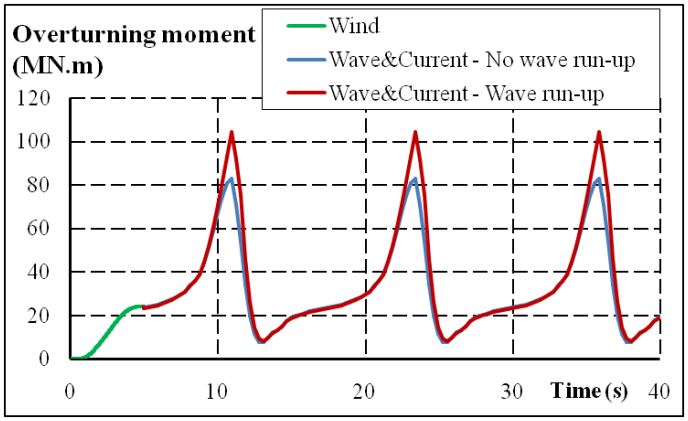

Figure 11. Meteorological mast global overturning moment at the seabed.

Figure 12 presents the stress extracted from two highly stressed areas: the lattice tower leeward chord at the connection to the platform and the monopile at the seabed. In Fig. 12, it can be observed that the wave crests at approximately t = 24 s and 37 s generated large stress variations in the tower, whereas the monopile stress varied consistently with the wave load profile. The rapid stress variations in the tower were induced by the global vibration of the tower after the sudden wave crest load release. The tower vibration can also be observed in Fig. 13 that shows the lateral displacement of the top of the tower over the time. The shortness of the transition from the wave maximum to minimum loads ~1.5 s observed in Fig. 12 can explain the dynamic response of the tower structure which the 1st mode natural period (i.e. 1-node bending) is around 1.6s. In Fig. 12, it appeared also that the maximum stress in the tower was significantly affected by the wave run-up consideration that increased the maximum stress by approximately 156%, whereas the rise of maximum stress in the monopile was consistent with the increase of maximum overturning moment presented in Fig. 11, approximately 120%.

Finally, the dynamic effect of the wave and the added contribution of the wave run-up load had a significant influence on the tower structural response which the stress at the leeward leg connection to the platform raised by 180% compared to the constant wind load response (see Fig. 12, left). Therefore, the ultimate strength of monopile-supported units should be verified under dynamic wave loads finite element analysis including the wave run-up component.

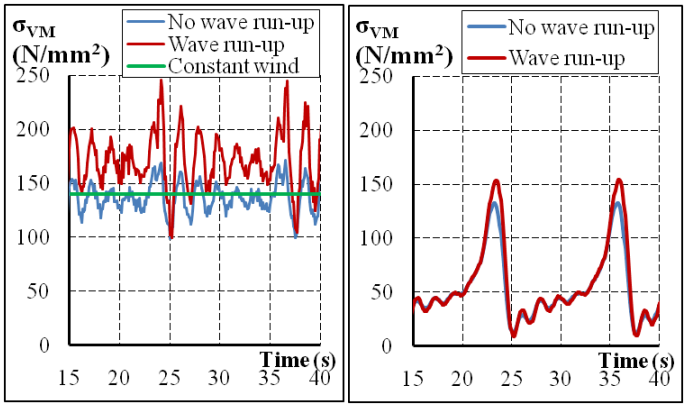

Figure 12. Maximum Von Mises stress on the lattice tower leeward chord at the connection to the platform (right) and on the monopile at the seabed (left).

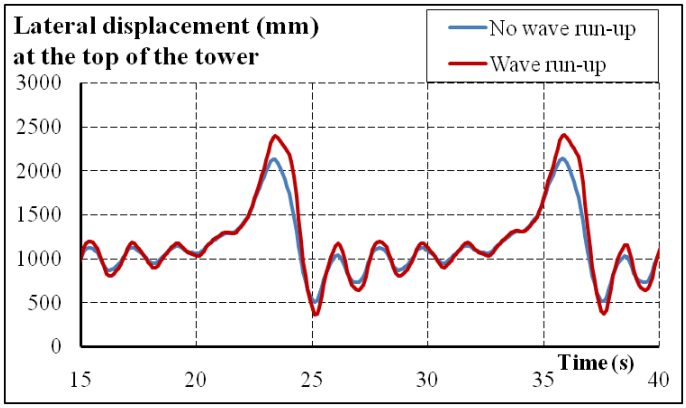

Figure 13. Lateral displacement at the top of the tower.

Wind load on parked wind turbine with blade pitch control fault

The blade pitch control fault effect on the parked wind turbine dynamic structural response was here analyzed. Figure 14 presents the global overturning moment at the seabed

exerted by the environmental loads while the turbine is parked with and without fault condition. At first, the constant wind load was applied through a 5 s preload step. The dynamic wave loads were then applied during three wave periods.

Figure 15 shows the stress in the leeward leg of the jacket at the pile-leg connection for the two load cases. In Fig. 15, it can be observed that the stress evolution was consistent with the exerted load variations. Therefore, the dynamic effect of the wave was not significant. It appeared also that for the fault condition, the stress increased by approximately 220% compared to the parked without fault condition. Therefore, designing wind turbine foundation for this extreme load case would require significant structure reinforcement.

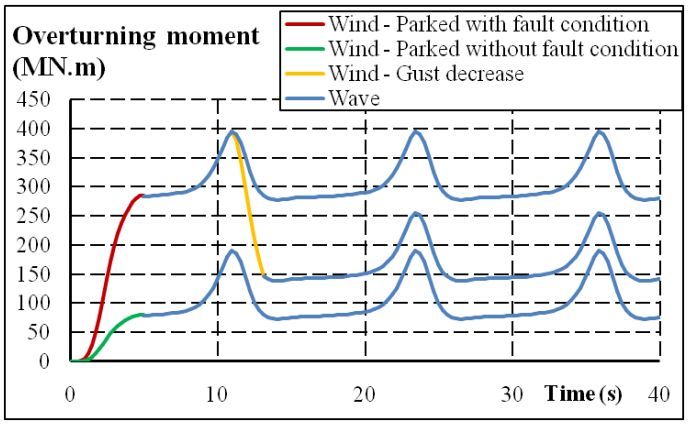

Figure 14. Wind turbine global overturning moment at the seabed.

The wind load dynamic effect should also be considered in this load case to include the rapid variation of wind speed and direction during the gust. Gust wind decrease analyses were thus conducted that simulated the wind load rapid drop from a 70 m/s gust wind speed to a 50 m/s mean wind speed for a transition duration ranging between 1 s and 6 s. Figure 14 presents a "gust decrease" the global overturning moment at the seabed exerted by the environmental loads for the parked wind turbine with blade pitch control fault. Figure 16 shows the nacelle horizontal displacement for various durations of gust wind drop. For gust drop duration under 3 s, significant dynamic oscillations can be observed, whereas above 3 s duration, the structure response was quasi-static. The threshold 3 s duration was consistent with the first natural period of the wind turbine (i.e. 1-node bending) approximately equal to 3.3 s. Therefore, especially for dynamic gust wind load cases considering the parked with fault condition, the FE model should reproduce accurately the wind turbine 1st natural modes to evaluate accurately the gust-induced dynamic response.

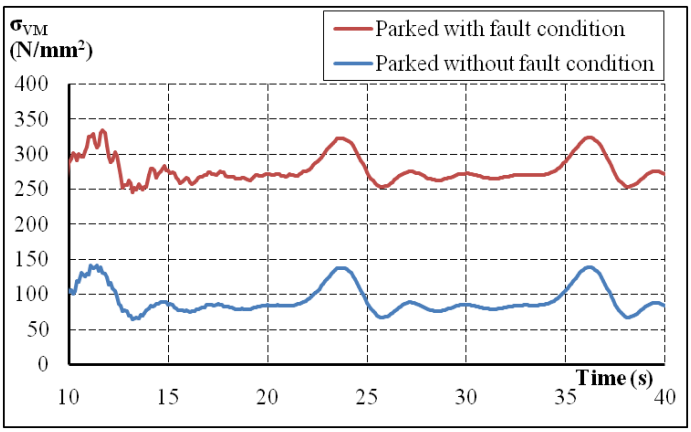

Figure 15. Maximum Von Mises stress in the leeward leg of the jacket at the pile connection for the two load cases.

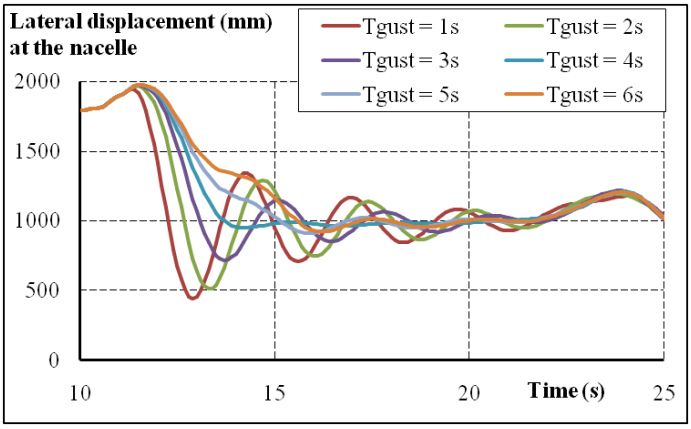

Figure 16. Lateral displacement at the nacelle during gust rapid drop.

CONCLUSIONS

This study evaluated the extreme typhoon loads acting on two offshore wind units: a meteorological mast and a wind turbine. The design environment considered a 14.9 m maximum wave height in a 25 m extreme water depth combined to collinear constant gust wind speed of 70 m/s and surface current speed of 1.4 m/s. This study investigated two critical load cases namely the dynamic wave run-up on a monopile foundation and the wind load acting on a parked wind turbine with blade pitch control fault. For each critical load cases, finite element analyses were conducted to evaluate the dynamic structure response of the considered units.

First, this study provided a semi-analytical model that enabled evaluating the wave run-up loads on monopile foundation. The model consisted in adding to the Morison equation a run-up induced slamming load term which the parameters were calibrated based on CFD analyses. For the considered meteorological mast, the slamming load consideration increased the global overturning moment by approximately 20% compared to the non slamming load calculation. Regarding the structure response, the stress increase

in the monopile induced by the consideration of the slamming load was consistent with the rise of overturning moment so that no significant dynamic effect was observed. However, for the meteorological tower mounted on top of the monopile, the dynamic effect of the wave load combined to the run-up induced slamming load generated a huge increase of the maximum stress of approximately 180% compared to the static response of the tower obtained at the end of the constant wind preload step. In addition, large stress variations and top of tower lateral displacement oscillations were observed after the wave crest passage, which indicated a global vibratory behavior of the tower. The dynamic run-up load was thus recommended to verify the strength of monopile supported units.

This study evaluated then the extreme wind load acting on the blades of the parked wind turbine with blade pitch control fault that would prevent reducing the blade projected area normal to the direction of the wind, inducing extremely high loads at the nacelle. The wind load exerted on the blades was computed using the blade element momentum (BEM) method. However, because the blades detailed design of the considered 3.6MW turbine was not available, an inverse calculation technique was employed to deduce an estimated geometry of the blades sufficient to compute extreme loads. The BEM method was validated by reproducing accurately the power curve of a 2.0 MW wind turbine. The inverse calculation enabled providing blades modeling that produced extreme load evaluation in agreement with the design extreme load provided by the manufacturer. Eventually, for the parked wind turbine with fault condition, the load raised by 350% compared to the normally parked condition. However, the tremendous increase of load on the parked wind turbine with fault condition would require significant structure reinforcements and thus additional cost, so that for typhoon-prone areas the addition of a backup system such as an emergency generator fitted in the nacelle would enable preventing this kind of system malfunction reducing significantly the severity of the design loads. Besides, the stress variations in the jacket foundation were consistent with the overturning moment variations, so that the wave-induced dynamic structure response was negligible, whereas the jacket dynamic structure response to the gust wind speed sudden drop was significant, especially for wind speed drop duration less than the 1st mode natural period of the structure ~3.3 s. An accurate structure FE modeling is thus required in order to reproduce accurately the structure dynamic response during extreme gust event.

To conclude, this study provided simplified load evaluation models that can produce realistic extreme design loads in typhoon condition with limited data. In the future, the validation of the load evaluation approaches should be carried out based on full scale measurements of wind speed, wave height and structure accelerations.

ACKNOWLEGMENTS

The authors would like to acknowledge Fuhai Wind Farm Corp. for providing us information regarding the design of the investigated offshore wind units.

REFERENCES

[1] Ministry of Economic Affair of Taiwan (R.O.C.), "風力發電離岸系統示範獎勵辦法(Regulations for Demonstration and Rewards of Offshore Wind Power System)." Taiwan (R.O.C.), 2012.

[2] P.C. Chang, R.Y. Yang, C.M. Lai, "Potential of Offshore Wind Energy and Extreme Wind Speed Forecasting on the West Coast of Taiwan." *Energies*, 2015 , 8, 1685-1700.

[3] A. Khansari, H. Oumeraci, "An overview of the dynamic response of jacket structure under breaking and non-breaking wave loads." *34th International Conference on Ocean, Offshore and Arctic Engineering*, No. OMAE2015-41976, 2015.

[4] "Environmental Conditions and Environmental Loads – Regular wave theories," *DNV-RP-C205*, Sec. 3.2, Oct. 2010.

[5] J.R. Morison, M.P. O'Brien, J.W. Johnson, S.A. Schaaf, "The force exerted by surface waves on piles." *Petroleum Transactions*, Vol. 189: pp.149-154, 1950.

[6] "Design of Offshore Wind Turbine Structures – Wave loads," *DNV-OS-J101*, Sec. 4.5.4, May 2014.

[7] J.F. Manwell, J.G. McGowan, A.L. Rogers, "Wind energy explained: theory, design and application." *Wiley*, Chichester, U.K., 2009

[8] D.M. Pitt, D.A. Peters, "Theoretical Predictions of Dynamic Inflow Derivatives." *Vertica*, 1981.

[9] AMC Portal of Wind Park Tai-Chung Power Plant, "Zephyzos Z72 wind turbine – Technical and Performance Data." *Taiwan Power Company*, 1981.

[10] "Design of Offshore Wind Turbine Structures." *DNV-OS-J101*, Appendix F, May 2014.

[11] "Design of Offshore Wind Turbine Structures – Load factors for the ULS," *DNV-OS-J101*, Sec. 5.1.1, May 2014.

[12] De Vos, L., Peter Frigaard and Julien De Rouck., "Wave Run-Up on Cylindrical and Cone Shaped Foundations for Offshore Wind Turbines," *Coastal Engineering Journal*, Vol.54.1, pp. 17-279, 2007.

[13] Ramirez, J., P. Frigaard, T.L. Andersen and L. de Vos, "Large Scale Model Test Investigation on Wave Run-Up in Irregular Waves at Slender Piles," *Coastal Engineering Journal*, Vol.72, pp. 68-79, 2013.

[14] Hallermeier, R.J., "Nonlinear Flow of Wave Crests Past a Thin Pile," *Journal of the Waterways Harbors and Coastal Engineering Division-Asce*, Vol.102, pp. 365-377, 1976.

[15] J.D. Fenton, "Nonlinear Wave Theories," *The Sea, Ocean Engineering Science*, Vol. 9, 1990, New York.

[16] Rupp Carriveau, "Fundamental and Advanced Topics in Wind Power," Published by *InTech*, Free online ed., June 2011, .